# Influence of radiation damage on perturbed angular distributions: The Po*Pb* system

E. Dafni,* M. H. Rafailovich, W. A. Little,† and G. D. Sprouse
*Department of Physics, State University of New York, Stony Brook, New York 11794*
(Received 28 March 1980)

Perturbed angular distribution measurements in a Pb target have been performed for the $^{206,208,210}$Po($8^+$) and $^{209}$Po($17/2^-$) isomeric levels. Target temperatures were varied from 80 to 575 K and magnetic fields were applied from 0.1 to 6.1 T. The data can be explained with a combined strong magnetic and weak quadrupole interaction, with the quadrupole interaction arising from radiation damage in the host correlated in position with the implanted ion. A perturbation theory treatment of the combined magnetic and quadrupole interaction was developed and provides the basis for the interpretation of the results. The data are consistent with a Lorentzian distribution of electric field gradients centered around zero with half width $\Gamma/2 = 0.9\times10^{17}$ V/cm$^2$ at room temperature. At higher temperatures the gradients are weaker indicating that before the measurement begins at $10^{-8}$ sec after the implantation, some annealing of the initial damage takes place.

[NUCLEAR REACTIONS $^{204,206,207,208}$Pb($\alpha$, $2n$)$^{206,208,209,210}$Po*, $E$ = 24–25.5 MeV. Enriched targets measured $\sigma(E_\gamma; \theta, H, t, T)$ for isomeric levels. Deduced electric field gradients from radiation damage.]

## I. INTRODUCTION

The study of angular distributions of $\gamma$ rays from the decay of high-spin levels is an important tool for the construction of level schemes and for spin assignments. Since high spin levels are often isomeric, their static electromagnetic moments can be measured using the perturbed angular distribution (PAD) method. In many cases, undesired perturbations are present along with the applied fields, and observation of the nuclear precession or the unperturbed angular distribution is impossible. In particular, our understanding of the perturbations from electric field gradients (EFG) caused by lattice defects in a metallic host is very limited.

Since heavy ion (HI) reactions produce large recoil momenta, much damage is created in the vicinity of the recoiled probe nuclei. This damage is referred to as "correlated radiation damage" in contrast to uncorrelated damage which may be distributed randomly in the target volume by the beam. In many cases, the EFG from radiation damage results in the loss of the nuclear alignment before the observation starting time. Thus, the study of the interaction between nuclei and radiation damage is very important from the nuclear physicist's point of view. An understanding of the damage distribution, migration, and annealing processes can assist in finding unperturbed environments for spin and moment measurements in cases where it was impossible before.

The objective of the present work was to define the conditions for preservation of the nuclear alignment for the polonium in lead (Po*Pb*) system and to understand the dealignment mechanisms involved. This system was chosen for several reasons. Lead has been used in the past as a host for time differential perturbed angular distribution (TDPAD) experiments, including fission isomer studies. The cubic structure provides a symmetric environment to the implanted Po nuclei and no EFG from the host lattice is present for the most likely substitutional site. Since lead is a well-studied metal, our results can be correlated to known solid state information. In addition, the Po isotopes offer isomeric states with a range of convenient lifetimes. The isomeric ($8^+$) states in $^{206,208,210}$Po and the $\frac{17}{2}^-$ state in $^{209}$Po have almost identical $g$ factors but different electric quadrupole moments, and they are easy to populate by ($\alpha$, $2n$) reactions with different enriched lead isotopes as targets.

### A. Preliminary work and a model

In preliminary experiments, the $^{208}$Po($8^+$) and $^{210}$Po($8^+$) isomers were implanted into a lead target, and the spin rotation patterns in the presence of an external magnetic field were observed for different target temperatures.[1] Some spectra of $^{208}$Po($8^+$)*Pb* at different target temperatures are shown in Fig. 1. The experiments and analysis are described in detail in Sec. II. It is seen that at temperatures lower than 575 K, less than the complete initial alignment is observed. At all temperatures, but in particular at the lower ones, there is damping of the alignment on a time scale of $\approx10^{-6}$ sec. Such damping may arise in paramagnetic systems from fluctuating magnetic hy-

 

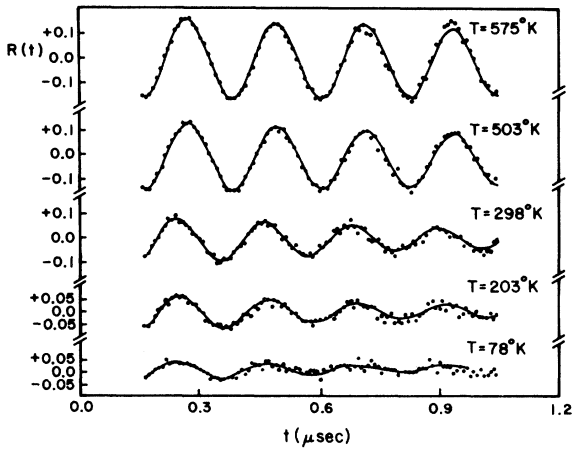


FIG. 1. Spin rotation spectra for $^{208}$Po($8^+$) in Pb for different temperatures. $R(t)$ is defined in Eq. (4). The magnetic field was nominally 0.3 T and was slightly different for the cooling and heating devices.

perfine fields at the probe site. However, Po is not expected to be paramagnetic in lead, and indeed the Larmor frequencies are independent of the temperature while such dependence exists in paramagnetic systems. A fluctuating field can also arise from possible defect motion, and Heubes *et al.*[2] have interpreted their spectra of $^{210}$Po in Pb with a fluctuating EFG. However, in our best data, one can distinguish that the damping is not exponential as it would be in a fluctuating field model, and we have rejected this mechanism for the dealignment. An alternative explanation for the damping of the spin rotation pattern is that of static, randomly oriented EFG's from frozen radiation damage combined with the external magnetic field. This explanation is supported if we consider the migration rate of point defects in lead. Self-interstitials are very mobile in the temperature range of the present experiments ($T > 80$ K) and, most probably, should not be considered in our system at all. Defects of importance are, then, monovacancies or small clusters of vacancies. The migration energy of a vacancy in lead[3,4] is $E_M = 0.56 \pm 0.13$ eV. Migration energies of polyvacancies are of the same magnitude or slightly smaller. The jump frequency of a vacancy in the lattice is given by

$$\nu = \nu_0 e^{S_M/k} e^{-E_M/kT}, \tag{1}$$

where $S_M$ and $\nu_0$ denote the entropy of migration and the attempt frequency associated with the jump, respectively. For lead,[4,5] $S_M = 0.7 \pm 0.2$ K and $\nu_0$ is $1.51 \times 10^{12}$ Hz. Using these numerical values, we obtain

$$\nu \approx 3 \times 10^{12} \times \exp(-6500/T)(\text{sec}^{-1}). \tag{2}$$

For temperatures below $\approx 450$ K, vacancies are frozen during the time scale of the present experiment ($\approx 10^{-6}$ sec). At the highest temperature used in this study, 575 K, vacancies jump every 25 nsec on the average.

Because of the presence of the defects in the vicinity of the probe nucleus, a combined magnetic and quadrupole interaction is applied to the probe. A complete calculation of the angular distribution with combined magnetic dipole and static electric quadrupole interactions is not available for high spins. It has been shown[6] using a first order perturbation calculation that for weak EFG's the combined interaction results in a Gaussian shaped envelope to the Larmor oscillations. The experimental observation of loss of initial alignment and damping can then be explained in the following way. After the nuclear reaction, the recoil nucleus is stopped in an environment characterized by a high density of lattice defects and a very high degree of lattice excitation which is dissipated in times of the order of $10^{-11}$ sec.[7] During this period, damage annealing takes place and the more mobile damage (interstitials) migrates away to regions of lower defect concentration. After the environment of the impurity is deexcited, a certain amount of damage is still located near the impurity. These static lattice defects give rise to EFG's which interact with the nuclear quadrupole moment. For a given target temperature there will then be a quadrupole interaction strength distribution $P(\omega_Q)$, where $P(\omega_Q) \times d\omega_Q$ is the fraction of Po nuclei subject to the quadrupole frequency between $\omega_Q$ and $\omega_Q + d\omega_Q$. A schematic drawing of a possible $P(\omega_Q)$ distribution is shown in Fig. 2.

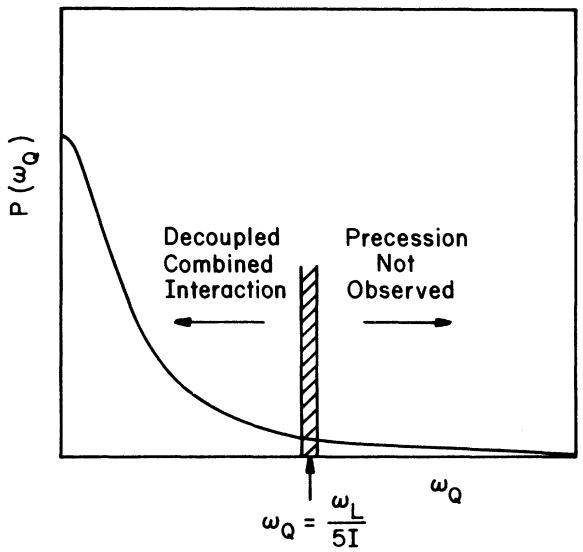


FIG. 2. Schematic representation of a possible distribution of electric field gradients.

For the fraction of Po nuclei for which the magnetic interaction is much stronger than the quadrupole interaction, the Larmor oscillations are observed but are confined to a Gaussian envelope, the width of which is related to an average quadrupole interaction strength. For the other fraction of Po nuclei with electric interactions larger or comparable to the magnetic interaction, no Larmor oscillations are observed after a sufficient time. We explain the loss of initial alignment as a result of strong EFG's which remove a fraction of the Po nuclei from the Larmor precession. The observed damping is a result of weak EFG's interacting with the rest of the Po nuclei. For a given EFG distribution, the fraction of probe nuclei for which the electric interaction is weaker than the magnetic interaction is a function of the nuclear $g$ factor, the external magnetic field, and the nuclear quadrupole moment. Experiments to measure the magnetic field dependence, the quadrupole moment dependence, and the target temperature dependence of the observed alignment have been performed and are discussed below, in the framework of the above model.

### B. The Po isomers

Isomeric states are known to exist in different Po isotopes from $A=202$ to $A=212$. Four of these isomers, the $(8^+)$ states in $^{206,208,210}$Po and the $\frac{17}{2}^-$ state in $^{209}$Po, were used as probes in the present study. These four isomers were first reported by Yamazaki[8] and they were chosen here for their suitable lifetimes and their ease of population with available beams and targets. The magnetic moments of the isomers were further studied by Nagamiya *et al.*[9] Häusser *et al.*[10] have reported precise $g$-factor and lifetime measurements for $^{208,209,210}$Po. The decay schemes of $^{206,208,209,210}$Po are displayed in Fig. 3.

The $8^+$ states of the even mass isotopes are the highest members of the $(h_{9/2})^2$ proton configurations. Their $g$ factors are equal to the $g$ factor of the $h_{9/2}$ ground state in $^{209}$Bi except for small corrections.

In order to estimate the quadrupole moment of the even Po isomers we make the following assumptions.

(i) The wave functions consist of

$$|8^+\rangle = |\pi(h_{9/2})^2 8^+\rangle$$
$$|6^+\rangle = |\pi(h_{9/2})^2 6^+\rangle .$$

The effects of the other contributions to the wave functions will then be included in the $E2$ effective charges.

(ii) Within the same nucleus the static $E2$ effective charges for protons in the $(h_{9/2})^2$ $8^+$ configuration are the same as for the transition effective charges which appear in the $B(E2)$ $[8^+ \rightarrow 6^+]$. This assumption was found to be correct in the Pb isotopes[11] as well as in the Mo isotopes[12] in the region of the $^{90}$Zr core. A relation between the static electric quadrupole moments of the $8^+$ state and the $B(E2)$ $[8^+ \rightarrow 6^+]$ value can then be derived, i.e.,

$$|eQ| = 6.19\,|B(E2)|^{1/2}\ e\,\mathrm{fm}^2 . \qquad (3)$$

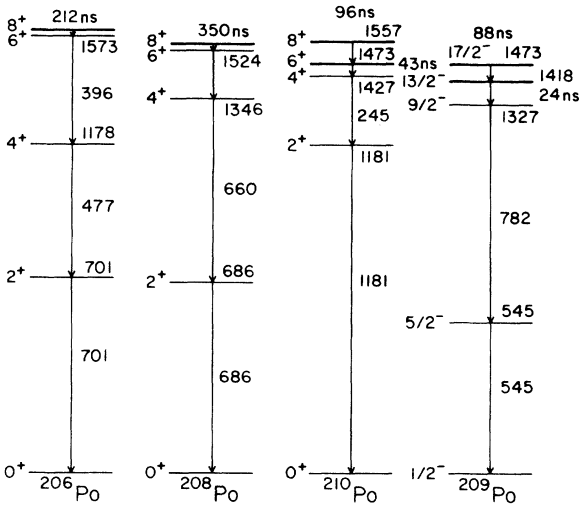


FIG. 3. Level schemes of the Po isotopes used in this work.

The similarity between the energy levels of $^{209}$Po and $^{208}$Po suggests the $|\pi(h_{9/2})^2\ 8^+ \otimes \nu p_{1/2}\rangle$ structure for the $^{209}$Po$(\frac{17}{2}^-)$ state, and Eq. (3) then also holds for $^{209}$Po, as the $p_{1/2}$ neutron does not contribute to the moment or the transition in first order.

In addition to the radiative decay of the $8^+$ states, internal conversion[13] of the low energy $E2$ transitions is an important deexcitation process. The half-life measurement can be used to extract the $B(E2)$ values even when the transition energy is not exactly known, as the conversion emission probability is rather insensitive to the transition energy. For $^{210}$Po and $^{209}$Po the transition energies are known and the $B(E2)$ values can be evaluated. For $^{208}$Po, this energy is believed to be less than 14 keV, and it is unknown for $^{206}$Po. Two $B(E2)$ values may be derived for the case of $^{206}$Po, depending on whether the transition is above or below the threshold for $L$ conversion. The higher value (see Table I) is favored since the quadrupole moment is expected to increase as we go further away from the closed neutron shell.[11] The ratio between the quadrupole moments of $^{206}$Po and $^{208}$Po was measured experimentally by Feilitzsch *et al.*[14] as $Q[^{206}\mathrm{Po}(8^+)]/Q[^{208}\mathrm{Po}(8^+)] = 1.3(1)$ in agreement with the higher value (1.3 for $E_\gamma < 14$ keV). All of

TABLE I. Po isotopes used in the present work.

| Nucleus | Isomer energy (keV) | Spin parity $J^\pi$ | $g$ factor (uncorrected) | $T_{1/2}$ (nsec) | $E_\gamma[J^\pi \rightarrow (J-2)^\pi]$ (keV) | $B[E2; J^\pi \rightarrow (J-2)^\pi]$ ($e^2$ fm$^4$) | $eQ$ ($e$ fm$^2$) |
|---|---|---|---|---|---|---|---|
| $^{210}$Po [a] | 1557 | $8^+$ | 0.914(1) | 96.0(14) | 83.6 | 85 | 57 |
| $^{209}$Po [a] | 1473 | $\frac{1}{2}^-$ | 0.907(1) | 88.5(15) | 55 | 111 | 65 |
| $^{208}$Po [a] | $1524+x$ | $8^+$ | 0.919(1) | 350(20) | <15 | 114 | 66 |
| $^{206}$Po [b] | $1573+x$ | $8^+$ | 0.915(13) | 212(5) | <14 | 189 | 85 |
| | | | | | >14 | 47 | 42 |

[a] Reference 9.
[b] Reference 8.

the known electromagnetic properties of the Po isomers are summarized in Table I.

## II. EXPERIMENTAL PROCEDURE

### A. Apparatus and techniques

All the experiments performed were spin rotation measurements, using the TDPAD method with pulsed $\alpha$-particle beams. As this method is discussed in detail elsewhere,[15] we will only point out details which are specific to the present work.

(a) *Beams and reactions.* Pulsed $^4$He beams of energy 24–25.5 MeV were obtained from the Stony Brook FN Tandem. The beam bursts were bunched in time to full width at half maximum (FWHM) $\approx$ 1.5 nsec, and the repetition time was 1–4 $\mu$sec, depending on which isomer was studied. The beam intensity was typically several nanoamperes, and was sometimes reduced to limit the detectors' counting rate.

(b) *Targets.* Thick isotopically enriched Pb foils were used in all experiments and the beams were stopped in the targets. The isotopically enriched targets were difficult to obtain with extremely high chemical purity. To ensure that differences in the chemical nature of the host did not affect our measurements, we populated several isomers in a mixed target and also in a 99.99% pure natural Pb target. The results obtained at room temperature and a field of 0.3 T were in agreement with the results from the isotopic targets to within the statistical errors.

(c) *Temperature control.* The targets were heated by a resistance heater consisting of a high resistance coaxial wire (Sodern Thermocoax) coiled around a copper block onto which the target was attached. Targets were cooled by means of a commercially available Joule-Thompson cooling device that was modified for in-beam experiments. In both cases the temperature was monitored using a thermocouple pressed against the target foil. The temperature measurement error results mainly from possible gradients between the beam spot and the thermocouple position and is estimated to be less than $\pm$5 K. A simple glass "$T$" was used as a target chamber in all experiments.

(d) *Detectors.* Two identical $\gamma$-ray detectors placed at $\pm$135° to the beam direction were used for most experiments. The detectors consisted of 5 cm long $\times$ 5 cm diam NaI(Tl) scintillators optically coupled to RCA 8575 photomultiplier tubes which were mounted on ORTEC 265 photomultiplier bases, and extensive magnetic shielding was employed. In the high magnetic field experiments with the in-beam superconducting magnet it was necessary to use 23 cm long light pipes between the detector crystals and the photomultiplier tubes. Time resolution of FWHM $\approx$ 2 nsec was typical for 511 keV $\gamma$ rays. Ge(Li) detectors were utilized for the mixed target experiment where the good energy resolution (typically FWHM $\approx$ 2.5 keV for 1.17 MeV $\gamma$ rays) was required.

(e) *Magnetic field.* An electromagnet, equipped with pole tips tapered to 5.1 cm diameter and with a 2.5 cm gap produced fields to 1.1 T. In this arrangement the field was homogeneous to $\approx$0.5% over the target size ($\approx$0.3 cm). The magnetic field was measured using a Hall probe which was calibrated in the 90° bending magnet of the accelerator. For higher field values, a superconducting magnet with fields up to 6.2 T was used, and the field was determined from the current in the magnet and from the known $g$ factor.

(f) *Electronics.* A schematic drawing of the electronics is shown in Fig. 4. Special care was taken to reduce dead time effects in the system. Since the time-to-amplitude converter (TAC) has a relatively long event processing time, the time signals were gated by the energy signals before the TAC was started. Time signals were delayed (by $\approx$2 $\mu$sec) until the energy analysis was carried out by the single channel analyzers (SCA). As

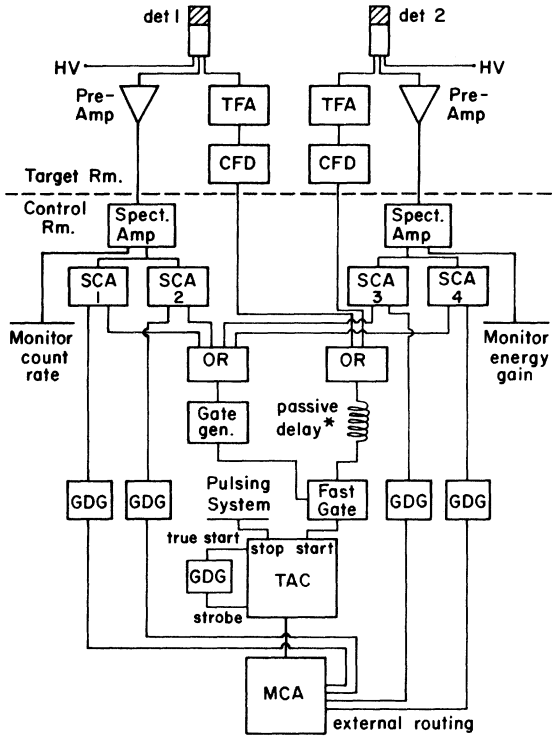


FIG. 4. Schematic drawing of the experimental electronics. The abbreviations are: HV—high voltage; TFA—timing filter amp; CFD—constant fraction disc.: SCA—single channel analyzer; GDG—gate and delay generator; TAC—time-to-amplitude converter; MCA—multichannel analyzer. Passive delay* is obtained by long cable. A fast amp is used every $\approx 0.5$ $\mu$sec.

active delay elements introduce their own jitter and dead time, this delay was achieved by sending the time signal through long cables. The pulse was rediscriminated every 500 nsec to overcome the attenuation and dispersion of the cable. The strobing time of the TAC was selected to produce a TAC dead time of $nt_0$-$\Delta$, where $n$ is an integer, $t_0$ is the beam repetition time (and also, normally, the TAC range), and $\Delta$ is typically 20–50 nsec. This procedure places any distortion effect from the TAC dead time after the intense prompt peak into the time range immediately before the prompt peak. The TAC output was recorded by a multichannel analyzer, and external routing was used to produce up to four different time spectra corresponding to different detectors or energies. The time scale was calibrated using the pulsing system reference oscillator.

(g) *Data manipulation.* The time spectra for a given $\gamma$ ray were fitted to a linear background plus an exponentially decaying term. The background was then subtracted and the spectra from the two detectors were normalized. In some cases, time spectra were collected for background $\gamma$ rays with energies near to the $\gamma$-ray energy window and these spectra were subtracted as background after a proper normalization. A ratio function $R(t)$ was then formed from the detectors' yield $Y_i(t)$

$$R(t)=\frac{Y_1(t)-Y_2(t)}{Y_1(t)+Y_2(t)}. \tag{4}$$

Several typical ratio functions are shown in Fig. 1.

### B. Experiments

While the previous section presented the experimental technique in a general manner, further specific details of the different experiments are given here. Although we are studying the perturbation of the isomeric levels, the $\gamma$ transitions which depopulate the isomers are difficult to observe because they are of low energy and highly converted. For different isomers it was advantageous to use different transitions, depending on the particular spectrum. The angular distribution is the same for all $\gamma$ rays in each stretched cascade, providing that no perturbation is present in the short lived intermediate states. The $^{210}$Po($6^+$) and the $^{209}$Po($\frac{13}{2}^-$) states are also isomeric but their lifetimes are short and their $g$ factors are almost identical to those of the higher spin isomers, so their calculated effect on the angular distribution with a pure magnetic interaction is negligible.[16] The effect of the intermediate states on the angular distribution with a combined magnetic and electric interactions has not been calculated. However, we estimate that the angular distributions observed in our experiments reflect essentially the perturbation due to the $8^+$ and the $\frac{17}{2}^-$ isomers, since the intermediate isomers have quadrupole moments of the same sign and similar magnitude as the higher spin isomers. The $^{210}$Po($8^+$) is the easiest Po isomer to populate. Both the 245 keV ($4^+ \rightarrow 2^+$) and 1180 keV ($2^+ \rightarrow 0^+$) $\gamma$ rays were observed for the $^{210}$Po measurement, and a sum of the counts in both $\gamma$ windows was used to generate the ratio functions. A beam energy of 24 MeV was used for all experiments except the high field measurements in the superconducting magnet where 25.5 MeV alphas were used. The measured alignment was independent of beam energy to within the errors.

The 447 keV ($4^+ \rightarrow 2^+$) $\gamma$ ray was observed for the $^{206}$Po measurements, and a combined 660 keV and 685 keV ($4^+ \rightarrow 2^+$, $2^+ \rightarrow 0^+$) energy window was used for $^{208}$Po. The $^{209}$Pb data was measured simultaneously with $^{208}$Pb, with a beam energy of 25.5 MeV, except for the measurements at 78 K, where

24 MeV was used because of accelerator limitations. The 782 keV ($\frac{9}{2}^- \rightarrow \frac{5}{2}^-$) $\gamma$ ray of $^{209}$Po was used for the time spectra. A background of this $\gamma$ ray exists in the $^{208}$Po time spectra. Since the $g$ factors and quadrupole moments of the two isomers are similar, a small contamination of the $^{209}$Po spectrum in the $^{208}$Po spectrum was not significant. Furthermore, the starting time of the $^{208}$Po observation ($\approx 175$ nsec) was after most of the $^{209}$Po isomers have been depopulated.

Measurements with different magnetic fields and different target temperatures were performed for the different isomers. The parameter space covered in the present work is shown in Fig. 5. The data were taken in many different runs. To check for systematic errors due to different electronic arrangements or different target properties, several points were repeated at different times. Agreement with statistical error was always observed.

### C. Data analysis

Our experimental system involves a combined transverse magnetic field and a randomly oriented electric field gradiant from radiation damage. An exact calculation of the angular distribution of $\gamma$ rays with this perturbation is possible, but requires much computer time for high nuclear spins. We have utilized the analytic functions of Ref. 6 which are appropriate for weak randomly oriented EFG and a strong magnetic field in order to fit the data. The basic formula is

$$W(\theta, t) = 1 + \sum_{k_1, k_2, N}^{k_{\max}} B_{k_1 k_2}^{NN} E_{k_1 k_2}^{NN}(I\omega_Q t) \cos[N(\theta - \omega_L t)], \tag{5}$$

where the notation is taken from Ref. 6. Note the decoupled form of Eq. (5). The $B$ coefficients contain all the geometrical information concerning the nuclear alignment and the radiation field properties. The envelope functions $E_{k_1 k_2}^{NN}(I\omega_Q t)$, shown in Fig. 6 for different spins, are independent of the magnetic field and contain the information about the electric interactions. These envelopes confine the usual Larmor oscillations to a decreased amplitude. It is apparent that these functions are almost independent of nuclear spin for $I\omega_Q t \leq 1$. A convenient estimate of the strength of a quadrupole interaction can be obtained by measuring the half-amplitude time of the observed envelope. For the dominant term $E_{22}^{22}$, half amplitude is reached for $I\omega_Q t = 0.63$, independent of $I$. We have fitted all ratio functions for the Po$Pb$ experiments to the function.

$$R(t)_{\text{comb}} = [B_{22}^{22} E_{22}^{22}(I\omega_Q t) + B_{24}^{22} E_{24}^{22}(I\omega_Q t)] \cos(2\omega_L t + \phi). \tag{6}$$

Implied in this parametrization is that we observe only those nuclei for which the magnetic interaction is strong compared to the quadrupole

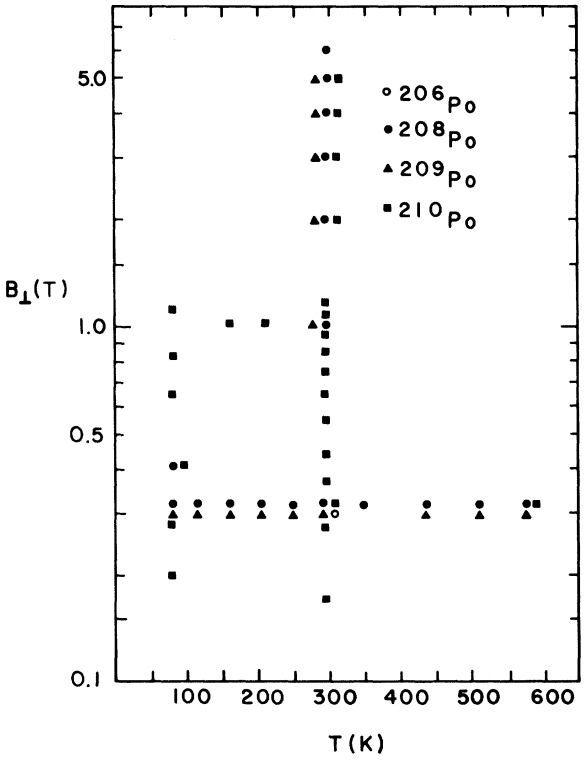


FIG. 5. Parameter space of the Po in Pb system covered in this work.

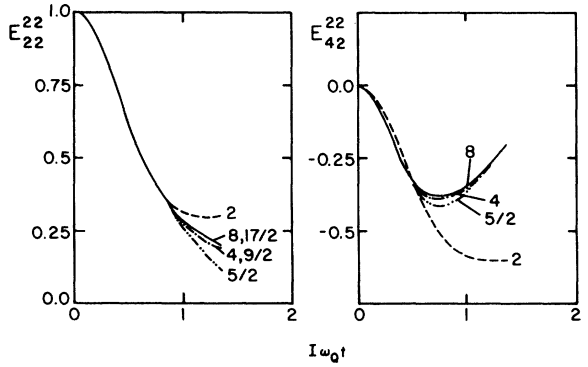


FIG. 6. Envelope functions $E_{22}^{22}$ and $E_{42}^{22}$, for different values of the nuclear spin I as a function if $I\omega_Q t$. Note the universal nature for $I\omega_Q t < 0.7$.

interaction. We denote the quantity[6] $\rho_2^* A_2$ as $a_2$, and since $\rho_4 \approx 0$, we have

$$B_{22}^{22} = \frac{3a_2}{4 + a_2}$$

and also[6]

$$B_{22}^{22} = -\left(\frac{15}{6}\right)^{1/2} \frac{A_4}{A_2}.$$

The free parameters in Eq. (6) are then: (i) $a_2$, the initial alignment, (ii) $\omega_Q$ and $\omega_L$, the quadrupole and the Larmor frequencies, respectively, and (iii) $\phi$, which depends on the detectors' angles, the $t = 0$ determination, and beam bending in the magnet. The fits started a fixed time $\Delta t$ after the prompt peak, in order to eliminate interference of the prompt peak and to allow for the decay of short lived background. This time was not changed for each isomer, in order to avoid systematic errors, but was different for the different isomers. The $\Delta t$ used for the $^{206,208,209,210}$Po isomers were 25, 175, 100, and 75 nsec, respectively. It was found that the fitting results depended on the starting time but were not sensitive to small changes in the ending time. The quoted values for the initial alignment $a_2$ have been corrected for finite solid angle and for finite time resolution.

## III. RESULTS AND DISCUSSION

### A. Magnetic field dependence

The magnetic field dependence of the initial alignment can be used to measure the strength of the quadrupole interactions from radiation damage and can help to determine the nuclear dealignment mechanism. The initial alignment for $^{208,209,210}$Po was studied at room temperature for fields up to 6.14 T. The data are shown in Fig. 7 Although the experimental error in the high field measurements is significant, an increase in alignment with increasing field is observed in all cases, in agreement with the assumption that as the field is increased, the decoupling condition is satisfied for a larger fraction of the nuclei.

The exact shape of the distribution of electric field gradients cannot be uniquely determined from the data. In order to fit the data, we have assumed a Lorentzian distribution of electric field gradients centered around $q = 0$.

$$L(q) = \frac{1}{\pi} \frac{\Gamma/2}{(\Gamma/2)^2 + q^2}, \tag{7}$$

where $\Gamma/2$ is the half width of the distribution. The

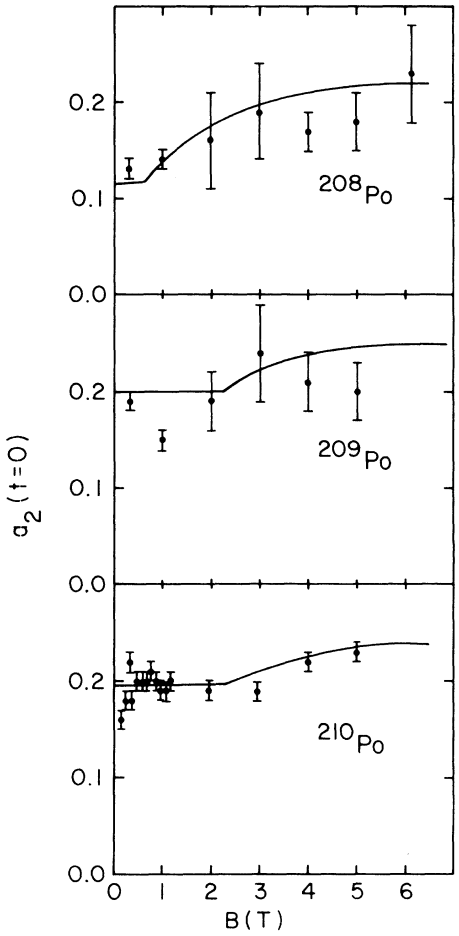


FIG. 7. Magnetic field dependence of the initial alignment parameter $a_2$ for different Po isomers. The smooth curves are fits to the data which are explained in the text.

fraction of nuclei, $f$, partaking in the Larmor precession is determined by

$$f = \int_0^{q_0} L(q)dq, \tag{8}$$

where $q_0$ is a cutoff parameter determined by the conditions of the measurement. Normally, $q_0$ is determined from the decoupling condition[6] $\omega_Q \geq \omega_L/5I$, and the observed $a_2$ increases as the field increases. At low fields, however, the observation time $\tau$ must be considered. To understand this dependence, consider a very short observation time, such as with a short lived isomer. For a weak gradient, one cannot discern until a time $\tau \geq 1/I\omega_Q$ whether the gradient is on or off. Therefore, we will always include in our integration those gradients weaker than $\omega_Q \leq 1/I\tau$. This gives rise to the flat portion of the curves in Fig. 7, which begin at different field levels for

different isomers. Reasonable agreement with the data is found for $\Gamma/2 = 0.9 \times 10^{17}$ V/cm$^2$. Other forms of the distribution was assumed and give fair agreement, but the long tail of the Lorentzian distribution is preferred to fit the gradual rise at higher fields. The sensitivity to small gradients of $^{208}$Po compared to the other isomers can be seen in the low field region of the data. The alignment is not destroyed for $^{209,210}$Po because the shorter measurement time is not sufficient to observe any of the weak quadrupole interactions.

### B. Quadrupole moment dependence

We have seen from the magnetic field dependence that increasing the magnetic field will include a larger fraction of nuclei in the Larmor precession. Conversely, increasing the quadrupole interaction strength should decrease this fraction of nuclei. The relative quadrupole moments of the $^{206}$Po and $^{210}$Po isomers is given by

$$Q[^{206}\mathrm{Po}(8^+)]/Q[^{210}\mathrm{Po}(8^+)] = 1.49 . \quad (9)$$

The spin rotation patterns for $^{206}$Po and $^{210}$Po in Pb were measured simultaneously using a natural lead target enriched to 20% $^{204}$Pb. The data are shown in Fig. 8. The target was held at $T = 293$ K and a transverse magnetic field of 0.32 T was applied. The least squares fits were done for the same time range for the two isomers. The fitting parameters are given in Table II, and we see that

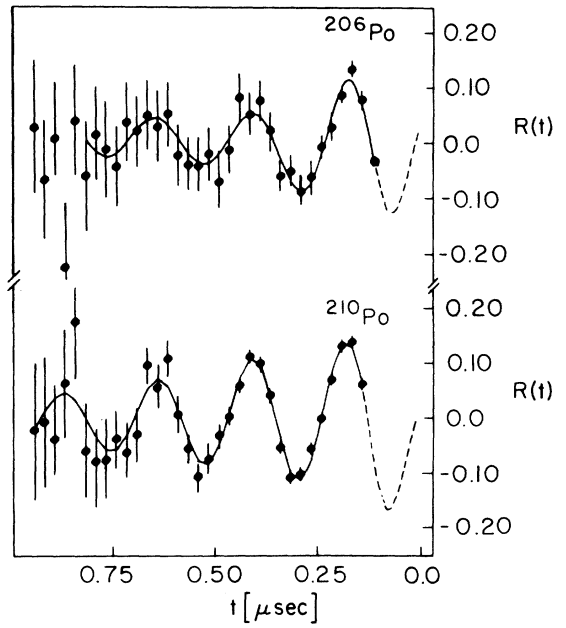


FIG. 8. Spin-rotation spectra for $^{210}$Po and $^{206}$Po at room temperature with a field of 0.32 T.

TABLE II. Parameters extracted from the natural Pb target at $T = 293$ K, $B = 0.32$ T.

| Isomer | $a_2(\Delta t)$ | $\overline{e^2qQ}/h$ (MHz) |
|---|---|---|
| $^{206}$Po(8$^+$) | 0.19(1) | 21(4) |
| $^{210}$Po(8$^+$) | 0.24(1) | 15(2) |

less alignment is observed for $^{206}$Po than $^{210}$Po.

The indication that the average quadrupole interaction strength scales linearly with the quadrupole moment is consistent with static perturbations, although the poor quality of the data does not rule out a quadratic scaling with the relative moments. Data were also taken for the $^{208}$Po(8$^+$) and $^{209}$Po($\frac{17}{2}^-$) isomers in the natural target. In this case, however, the quadrupole moments are very similar and it was not possible to observe any differences larger than the error involved in fitting the data.

### C. Temperature dependence

The magnetic field dependence and quadrupole moment dependence of the data taken at room temperature are consistent with a distribution of static electric field gradients being applied to the probe nuclei. The temperature dependence of the strength of these gradients can be used to investigate the dynamics of the annealing process on a time scale which is difficult to measure by classical radiation-damage techniques.

The most sensitive isomer for these studies is again the $^{208}$Po(8$^+$) because of its long lifetime. A field of 0.32 T was applied to the target. Spin rotation spectra at several temperatures are shown in Fig. 1, and the parameters extracted from these and other data are shown in Fig. 9. As the temperature is increased, the initial alignment increases, and the average gradient observed decreases in strength. The data are consistent with a distribution of gradients centered around zero strength whose width decreases steadily with increasing temperature.

We have characterized the distribution of EFG with a Lorentzian [Eq. (7)] and have adjusted the width of the distribution, $\Gamma$, with temperature as shown in Fig. 9(a) in order to simultaneously fit the data in Figs. 9(b) and 9(c). The smooth curve in Fig. 9(b) is generated with Eq. (8) and the curve in Fig. 9(c) is defined by

$$\overline{q(T)} = \int_0^{q_0} qL(q,T)dq . \quad (10)$$

The good agreement obtained simultaneously for both data indicate that the shape of the distribution of gradients is well fit by the Lorentzian. From

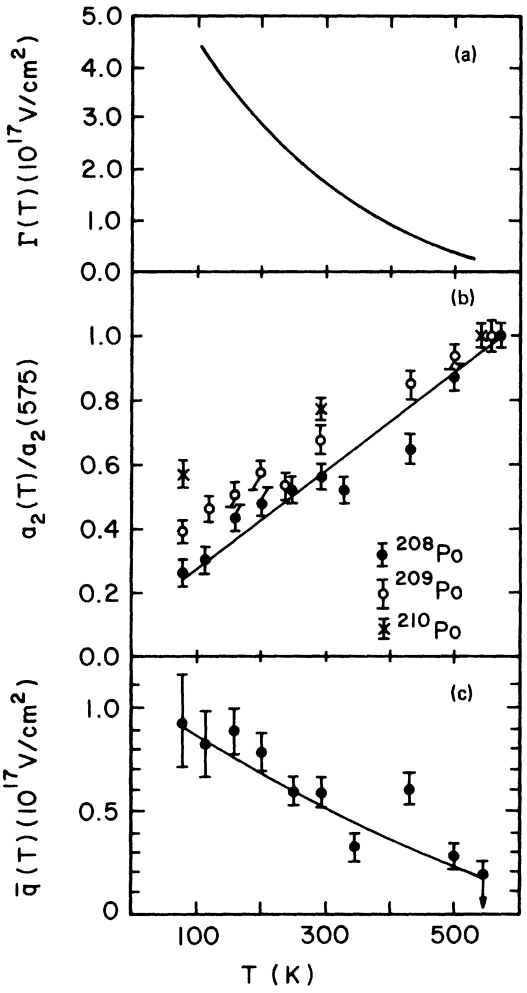


FIG. 9. (a) Width parameter Γ for a Lorentzian distribution of electric field gradients [derived from the data in (b) and (c)]. (b) Initial alignment parameter $a_2(T)$ (normalized to the highest temperature) for the different Po isomers. The maximum alignment observed for $^{208}$Po, $^{209}$Po, and $^{210}$Po was 0.23(1), 0.28(1), and 0.26(1), respectively. (c) The average gradient observed for $^{208}$Po at different temperatures. A gradient of $q = 10^{17}$ V/cm$^2$ corresponds to $e^2qQ/h = 15.9$ MHz. Sternheimer corrections have not been made.

Fig. 9(a), we see that at lower temperatures, higher average gradients are observed.

In Fig. 9(b), we have also included the initial alignment parameter $a_2(t)/a_2(575)$ for the other isomers. Both $^{209}$Po and $^{210}$Po exhibit more alignment at lower temperatures than the longer-lived $^{208}$Po. This systematic trend can in part be explained by the smaller quadrupole moment of $^{210}$Po, but in addition the decreased observation starting time for the shorter lived isomers introduces some systematic differences in the fitting of the data. The average gradients obtained from the other isomers is consistent with but not nearly as sensitive and accurate as those obtained from the $^{208}$Po data, and have not been included.

### D. Damage annealing

All of the PAD measurements are consistent with a Lorentzian shaped distribution of static electric field gradients acting on the probe nuclei, with stronger gradients at lower target temperatures. Since the initial damage profile should be essentially temperature independent, we must therefore conclude that before the observation starts, some annealing takes place at the higher target temperature because the observed gradients are weaker. We can exclude the possibility that the annealing is taking place during the observation time, as the spectra at long times cannot be fitted with an exponential decay of the alignment which would be caused by a fluctuating environment.

In order to estimate the effect of damage annealing on the angular distribution we take the following approach. Immediately after the implanted nucleus is stopped, the lattice is in a high degree of excitation. Let us suppose that after the probe comes to rest there is a defect in the $j$th neighbor shell surrounding the probe. We define $P_{ij}(n)$ to be the probability that after $n$ jumps, the defect will be in the $i$th neighbor shell. In a simple model with point defects and all jump directions equally likely in the defect's first neighbor shell, we can easily calculate $P_{ij}(n)$ from the geometry of the fcc lattice. We have limited the calculation to the first 6 neighbor shells, and effects of damage migrating into these 6 shells from the outside are neglected. Defect clusters and binding effects are not considered in this simple model. The $P_{ij}(1)$ coefficients under these assumptions are given in Table III. For higher $n$ values, $P_{ij}(n)$ are given in matrix notation as $P(n) = P(1)^n$. With these coefficients one can find the damage distribution after $n$ jumps, providing that the initial distribution is known. To further simplify the problem we assume a constant initial damage density $\rho$, and that the electric field gradients at the probe location resulting from a defect in the $i$th shell scales like $1/d_i^3$, where $d_i$ is the probe-defect distance. In this simple model, we will neglect screening effects. The initial average electric field gradient is then

$$q(0) = q_0 \rho \sum_i \frac{N_i}{d_i^3}, \tag{11}$$

where $N_i$ is the number of neighbors in the $i$th lattice shell and $q_0$ is the EFG from a defect which is a unit distance away from the probe. The

TABLE III. $P_{ij}(1)$ coefficients.

| $j$ \ $i$ | 1 | 2 | 3 | 4 | 5 | 6 | >6 |
|---|---|---|---|---|---|---|---|
| 1 | 0.417 | 0.167 | 0.333 | 0.083 | | | |
| 2 | 0.333 | | 0.333 | | 0.333 | | |
| 3 | 0.167 | 0.083 | 0.167 | 0.167 | 0.167 | 0.083 | 0.167 |
| 4 | 0.083 | | 0.333 | | 0.167 | | 0.417 |
| 5 | | 0.167 | 0.167 | | | | 0.667 |
| 6 | | | 0.250 | | | | 0.750 |

average EFG after $n$ defect jumps is

$$\overline{q(n)} = q_0 \rho \sum_{ij} \frac{P_{ij}(n) N_j}{d_i^3} . \tag{12}$$

Values of $\overline{q(n)}/\overline{q(0)}$ are independent of $q_0$ and $\rho$ and are shown in Fig. 10. For $n \geq 2$ we see that

$$\overline{q(n)} \approx \overline{q(0)}\, e^{-(n-1)/4} . \tag{13}$$

We find that a small number of defect jumps is sufficient to produce an almost complete annealing. The exponential dependence in Eq. (13) is a property of the lattice geometry [i.e., the $P_{ij}(n)$ coefficients] and is independent of the details of the initial damage distribution and the actual screening of the EFG from far away defects, although a slightly different slope would be obtained if we included more than 6 shells in our model calculation. Even though we do not know how many defect jumps occur before the damage becomes immobile we can now estimate that around four additional defect jumps are made during the longer time to immobilize the lattice defects when the target is held at room temperature rather than 80 K. This result follows from the observation that the average gradient at 80 K is about 3 times larger than that at 295 K. This kind of information is not available from classical radiation damage measurements and it would be interesting to use as a test of different theories of the short term dynamics of the radiation damage process.

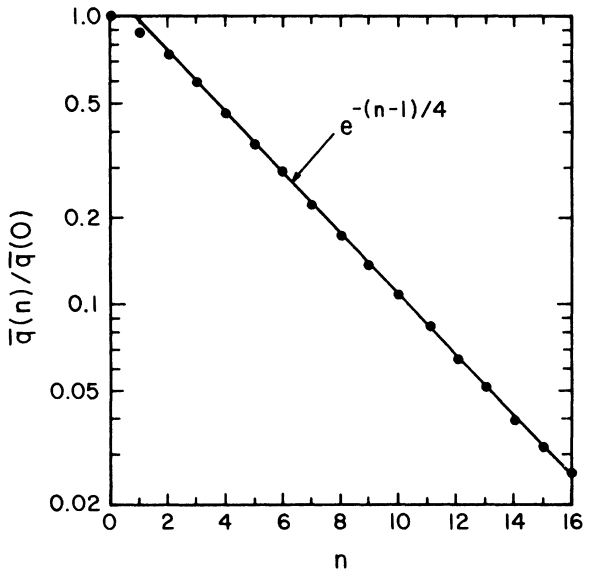


FIG. 10. Dependence of the average gradient $\overline{q}(n)$ on the number of defect jumps after implantation.

## V. SUMMARY

The loss of alignment due to solid state effects in one system, Po in Pb, has been studied in detail, in order to characterize this system as completely as possible, and to attempt a quantitative understanding of the dealignment mechanism, so that the results can be useful in interpreting other experiments, e.g., measurement of moments of fission isomers. The mechanism for the dealignment is consistent with a distribution of weak electric field gradients which are essentially static during the measurement time. The distribution at $T = 295$ K can be characterized with a Lorentzian distribution centered around $V_{zz} = 0$, with half width $\Gamma/2 = 0.9 \times 10^{17}$ V/cm$^2$. The observed gradients are consistent with point defects or defect clusters within several lattice spacings of the impurity probe nucleus.

The application of very strong magnetic fields does improve slightly the spin-rotation signal amplitude due to increased decoupling of the weak electric field gradients, but the amount of improvement does not justify the additional experimental difficulties of utilizing a superconducting magnet for the measurements. For measurements with fission isomers where the quadrupole moments are larger by over an order of magnitude, decoupling with strong fields does not seem to offer any promise to preserve the alignment if the gradients are of comparable magnitude for Pu in Pb as for Po in Pb.

The variation of the spin rotation spectra with temperature which were observed indicate that additional annealing takes place in the vicinity of the probe nucleus when the target is maintained at an elevated temperature than when the target is

held at low temperature. A simple model indicates that a defect takes approximately four more jumps within $10^{-8}$ sec after implantation when the target is at room temperature than when the target is at 80 K. This detailed information on the short time behavior of a damage cascade is not available by conventional radiation damage measurement techniques. The reputation of Pb as a "good" host for PAC measurements may be correlated with this annealing behavior. The energy of the damage cascade may be dissipated more readily into electronic degrees of freedom in a metallic host such as gold which is not a good host for PAC measurements, while the energy remains for a longer time in lattice degrees of freedom for lead, allowing some partial annealing of the lattice and consequently lower electric field gradient distributions. The observed behavior of the initial alignment for Po in Pb is qualitatively different from that observed for a large number of other systems.[17,18] In the Pb hosts, the alignment gradually increases with temperature, while in the other systems, a step is observed at about 60% of the melting temperature. This difference is probably another manifestation of different mechanisms for dissipation of the energy of the damage cascade in the different materials. There are many other parameters relevant to the loss of alignment in PAC measurements so that a complete quantitative explanation of these effects is not feasible at this time.

This work was supported in part by the National Science Foundation.

---

*Present address: Weizmann Institute, Rehovot, Israel.

†Present address: Grumman Aerospace Corporation, Ventura, California.

[1]E. Dafni, M. H. Rafailovich, W. A. Little, and G. D. Sprouse, Hyperfine Interactions 4, 743 (1978).

[2]P. Heubes, R. Keitel, W. Klinger, W. Loeffler, W. Sandner, W. Witthuhn, R. Langkau, and H. Krause, Hyperfine Interactions 4, 746 (1978).

[3]R. E. Hoffman, F. W. Pikens, and R. A. Ward, Trans. Metall. Soc. AIME 206, 483 (1956).

[4]R. Feder and A. S. Mourick, Philos. Mag. 15, 805 (1967).

[5]A. Seeger, H. Mehrer, in *Vacancies and Interstitials in Metals*, edited by A. Seeger *et al.* (North-Holland, Amsterdam, 1963).

[6]E. Dafni and G. D. Sprouse, Hyperfine Interactions 4, 777 (1978).

[7]P. Sigmund, Appl. Phys. Lett. 25, 169 (1974).

[8]T. Yamazaki, Phys. Rev. C 1, 290 (1970).

[9]S. Nagamiya, Y. Yamazaki, O. Hashimoto, T. Nomura, K. Nakai, and T. Yamazaki, Nucl. Phys. A211, 381 (1973).

[10]O. Hausser, T. K. Alexander, J. R. Beene, E. D. Earle, A. B. McDonald, F. C. Khanna, and I. S. Towner, Nucl. Phys. A273, 253 (1976).

[11]H.-E. Mahnke, T. K. Alexander, H. R. Andrews, O. Hausser, P. Taras, D. Ward, E. Dafni, and G. D. Sprouse, Phys. Lett. 88B, 48 (1979).

[12]C. V. K. Baba, D. B. Fossan, T. Faestermann, F. Feilitzsch, K. E. G. Lobner, and G. Signorini, Nucl. Phys. 48B, 218 (1974).

[13]R. S. Hager and E. C. Seltzer, Nucl. Data A4, 1 (1968).

[14]F. V. Feilitzsch, T. Faestermann, O. Hausser, K. E. G. Lobner, R. Lutter, H. Bohn, D. J. Donahue, R. L. Herschberger, and F. Riess, *Proceedings of the International Conference on Hyperfine Interactions Studied in Nuclear Reactions and Decay, Uppsala, Sweden, 1974*, edited by E. Karlsson and R. Wäppling (Uplands Grafiska AB, Uppsala, 1974).

[15]M. Morinaga and T. Yamazaki, *In-Beam Gamma Ray Spectroscopy* (North-Holland, Amsterdam, 1976).

[16]C. V. K. Baba, T. Faestermann, F. Feilitzsch, D. B. Fossan, P. Kienle, and C. Signorini, Phys. Lett. 43B, 483 (1973).

[17]G. Schatz and P. Heubes, Hyperfine Interactions 4, 751 (1978).

[18]G. Schatz, M. H. Rafailovich, W. A. Little, and G. D. Sprouse, Phys. Rev. Lett. 35, 1086 (1975).